

# Unveiling the Multifaceted Nature of 4-(4-Methylphenyl Thio)benzophenone: Electronic Structure and Excited States in Gas Phase and Solvents

Manjeet Bhatia<sup>\*[a]</sup>

Benzophenone and its derivatives are widely used as UV filters and UV-ink photoinitiators. The photoinitiating properties of benzophenones depend on their degree of conjugation and delocalization within the molecule. By understanding how conjugation, delocalization, and different substituents affect these properties, benzophenone derivatives can be customized for specific applications. Using quantum mechanical calculations based on B<sub>3</sub>LYP/6-311++G(d,p) density functional theory (DFT), chemical reactivity, stability, and photoinitiating capabilities of 4-(4-methylphenylthio)benzophenone are analyzed. This includes studying its physical and chemical properties in the gas phase, as well as its excited state electronic

transitions, vibrational characteristics, and spectroscopic properties both in gas phase and in various solvents. The DFT-computed infrared spectra match experimental results. The UV/Visible spectra shows absorption towards longer wavelengths due to extended delocalization of  $\pi$ -electrons. In different solvents with varying polarity, the absorption spectra exhibit high-intensity peaks, shift in excitation energy and wavelengths based on the polarity of the solvent. This knowledge allows for the development of novel initiators with customized light absorption, excited state lifetimes, and reaction selectivities, which can enhance processes like UV-curing, photopolymerization, and other light-driven reactions.

## 1. Introduction

Benzophenone-based photoinitiators are compounds derived from benzophenone that are used to initiate or catalyze chemical reactions when exposed to ultraviolet (UV) or visible light.<sup>[1,2]</sup> These photoinitiators are commonly employed in various applications such as photopolymerization, where they trigger the polymerization process upon exposure to light, leading to the formation of polymers or cross-linked networks. Benzophenone-based photoinitiators are particularly valued for their efficiency and versatility in initiating light-induced reactions in materials and coatings. Benzophenone based derivatives, with its simple yet elegant structure, boasts an almost magical ability to absorb light and undergo a transformation.<sup>[3]</sup> This excited state fuels a cascade of reactions, triggering the linking of monomers into intricate polymer chains. This remarkable capacity has propelled benzophenone and its derivatives to the forefront of photopolymerization technology, making them the most widely used class of photoinitiators.<sup>[4]</sup> Benzophenone initiates the curing of various resins and coatings (e.g., inks, adhesives, dental materials) upon exposure to UV light.<sup>[5,6,7]</sup> Benzophenone-based initiators can be incorporated into polymers to trigger their controlled degradation under specific light conditions. Benzophenone derivatives are being explored for photo-regulated drug delivery systems and photodynamic therapy due to their light-activated properties.<sup>[8,9]</sup>

The quest is on to tailor photoinitiators light absorption, enhance their efficiency, and restrain their unwanted wanderings within materials.<sup>[10,11]</sup> Conjugation and delocalization play a significant role in the photoinitiating properties of molecules by influencing their absorption of light, excited state stability, and reactivity. Conjugated molecules with alternating single and double bonds possess extended  $\pi$ -orbital systems. These delocalized  $\pi$ -electrons can efficiently interact with light of specific wavelengths, leading to stronger absorption in the UV or visible region. This increased light absorption is crucial for initiating photochemical reactions, as it triggers the initial excitation of electrons in the molecule. Delocalization of electrons across the conjugated system distributes the excitation energy over a larger area, stabilizing the excited state. This reduces the energy difference between the ground state and the excited state, making the molecule less prone to deactivation through non-productive pathways like fluorescence or internal conversion. Consequently, the excited state lives longer, increasing the probability of it participating in a desired photochemical reaction. Benzophenone and its derivatives remain the most widely used class of photoinitiators due to their effectiveness, broad absorption range, and relative affordability.<sup>[12,13,14]</sup> 4-(4-methylphenylthio)benzophenone (4-4-MPTB),<sup>[15,3,13]</sup> a classic photoinitiator whose conjugated  $\pi$ -system efficiently absorbs light and undergoes excitation, making it widely used in free radical polymerization reactions. Further, electron-donating or withdrawing groups attached to the conjugated system can further influence the light absorption and reactivity of the molecule. Modifying the benzophenone core with electron-donating or withdrawing groups to tune its excited state properties and reactivity. Identifying potential electrophilic, and nucleophilic sites, and  $\pi$ -electron

[a] Dr. M. Bhatia  
QuantumSIMM, 177105 Kangra, Himachal Pradesh, India  
E-mail: manjeetbhatia83@gmail.com  
Homepage: www.quantumsimm.com

delocalization are crucial for elucidating light absorption and reactivity of the molecule.

Furthermore, solvent effects on UV-Vis spectrometry can be observed through solvatochromic shift in the excited state electronic absorption spectra. This translates to stronger solvent-solute interactions, influencing shifts and intensity. These shifts and intensity changes arise from interactions between the solvent molecules and the solute's electron cloud. Solvents can stabilize or destabilize different excited states, altering their energy levels and consequently, the observed absorption spectrum.<sup>[16,17]</sup> Molecular properties along with global reactivity of 4-4-MPTB are computed using density functional theory (DFT) and conceptual DFT based on the response functions to the perturbation. These global reactivity descriptors are essential tools in theoretical chemistry, providing valuable information about a molecule's reactivity, stability, and electronic properties.<sup>[18,19,20]</sup>

The present article is organized as follows: Section 2 describes the computational method exploited to obtain optimized molecular geometry and other chemical properties. In section 3, DFT obtained results are discussed thoroughly. Finally, conclusions are given in section 4.

## Computational Method

The utilized hybrid DFT functional,<sup>[21]</sup> blends exchange contributions from Hartree-Fock theory with correlation contributions from DFT, achieving a commendable equilibrium between accuracy and computational efficiency across a diverse array of properties. It strikes a good balance between accuracy and computational cost for a wide range of properties, including: geometries, vibrational frequencies, thermochemical properties, electronic structure, e.g., highest occupied and lowest unoccupied (HOMO/LUMO) energies. B<sub>3</sub>LYP/6-311++G(d,p) method implemented on Gaussian 16 DFT code<sup>[22]</sup> is used to compute above molecular properties. It's a triple-zeta basis set with polarization functions on both heavy atoms (d) and hydrogen atoms (p). It provides a reasonable level of accuracy for many properties without being excessively computationally expensive. The “++” indicates that diffuse functions are added, which are essential for describing anions, long-range interactions, and excited states. To account for solvent effects on these properties, the polarizable continuum model (PCM) is employed within the Gaussian 16 software package. The PCM is a widely used continuum solvation model that treats the solvent as a continuous dielectric medium surrounding the solute molecule. Similarly, time-dependent density functional theory (TD-DFT) method is utilized to calculate UV/Vis spectroscopic properties of 4-4-MPTB molecule. The molecular structure is geometrically relaxed and vibrational frequency calculations confirmed that stationary point is found making sure that no imaginary frequencies are present. B<sub>3</sub>LYP/6-311++G(d,p) combination generally provides reliable results for a variety of molecular properties.<sup>[23,24]</sup> It is relatively efficient compared to more advanced functionals and basis sets applicable to a wide range of molecular systems and chemical phenomena.

## 2. Results and Discussion

### 2.1. Electronic Structure

Quantum mechanical calculations using B<sub>3</sub>LYP/6-311++G(d,p) DFT method implemented on Gaussian 16 suite of codes are exercised to obtain optimized molecular geometry of 4-4-MPTB. Then consecutive calculations, such as frequency, natural bond order (NBO), HOMO-LUMO, and spectroscopy are performed on the optimized geometry. The optimized structure of 4-4-MPTB is shown in Figure 1 and structural parameters are given in Table 1.

Table 2 presents the DFT-computed molecular properties, encompassing dipole moment, polarizability, proton affinity, ionization energy, electron affinity, and global reactivity parameters. The obtained results indicate a notable dipole moment (5.58 Debye) and substantial polarizability (40.24 Å<sup>3</sup>), highlighting their significance in elucidating intermolecular interactions and bonding characteristics within the molecule. In mass spectrometry drift tubes, the proton affinity and ionization energy play crucial roles in determining the nature and type of reactions.<sup>[25]</sup> Global reactivity parameters, including HOMO-LUMO energy, chemical potential ( $\mu$ ), chemical hardness ( $\eta$ ), softness ( $\sigma$ ), electrophilic index ( $\omega$ ), and electronegativity ( $\chi$ ) are computed as per Koopmans approximation.<sup>[26]</sup> Koopmans theorem assumes that if adding or removing an electron from a molecule preserves its electronic structure, then the ionization energy and electron affinity can be expressed as  $-\epsilon_{\text{HOMO}}$  and  $-\epsilon_{\text{LUMO}}$ , respectively. Koopmans approximation treats each electron as an independent particle, neglecting electron-electron correlations. Consequently, chemical reactivity parameters are derived from response functions based on orbital energies as outlined in previous studies.<sup>[27,28,29]</sup>

$$\mu = -\frac{1}{2}(\text{IP} + \text{EA}) = \frac{1}{2}(\epsilon_{\text{LUMO}} + \epsilon_{\text{HOMO}}) \quad (1)$$

$$\eta = \frac{1}{2}(\text{IP} - \text{EA}) = \frac{1}{2}(\epsilon_{\text{LUMO}} - \epsilon_{\text{HOMO}}) \quad (2)$$

$$\sigma = \frac{1}{2\eta} \quad (3)$$

$$\omega = \mu^2\sigma \quad (4)$$

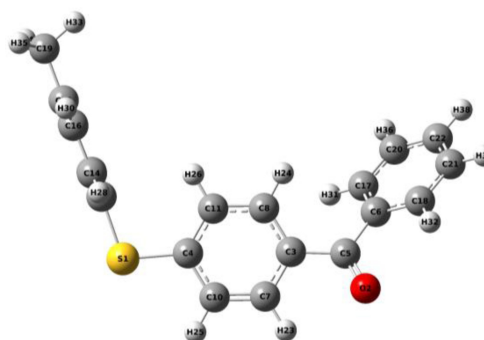


Figure 1. Fully optimized structure of 4-4-MPTB molecule from B<sub>3</sub>LYP/6-311++G(d,p) method.

**Table 1.** Optimized structural parameters of 4-4-MPTB using B<sub>3</sub>LYP/6-311 + +G(d, p) DFT method.

Bond	Length	Bond	Length	Bond	Angle	Bond	Angle
S1–C9	1.794	C10–H25	1.085	S1–C4–C10	116.3	C7–C10–H25	119.9
S1–C4	1.787	C11–H26	1.082	S1–C4–C11	124.4	C4–C11–C8	119.9
O2–C5	1.222	C12–C16	1.400	C10–C4–C11	119.3	C4–C11–H26	120.3
C3–C8	1.400	C12–C15	1.399	O2–C5–C3	120.3	C8–C11–H26	120.0
C3–C7	1.404	C12–C19	1.509	O2–C5–C6	119.6	C16–C12–C19	121.0
C3–C5	1.494	C13–C15	1.393	C3–C5–C6	120.2	C9–C13–C15	120.1
C4–C10	1.405	C13–H27	1.084	C5–C6–C17	122.6	C9–C13–H27	120.0
C4–C11	1.397	C14–C16	1.392	C5–C6–C18	118.1	C15–C13–H27	120.3
C5–C6	1.502	C14–H28	1.084	C17–C6–C18	119.1	C9–C14–C16	120.1
C6–C17	1.401	C15–H29	1.085	C3–C7–C10	120.9	C9–C14–H28	120.0
C6–C18	1.401	C16–H30	1.085	C3–C7–H23	118.6	C16–C14–H28	120.3
C7–C10	1.384	C17–H31	1.083	C10–C7–H23	120.4	C12–C15–C13	121.2
C7–H23	1.083	C17–C20	1.394	C3–C8–C11	121.1	C12–C15–H29	119.5
C8–C11	1.392	C18–H32	1.083	C3–C8–H24	120.1	C13–C15–H29	119.3
C8–H24	1.083	C18–H21	1.390	C11–C8–H24	118.8	C12–C16–C14	121.2
C9–C13	1.397	C19–H34	1.092	S1–C9–C13	120.2	C12–C16–H30	119.5
C9–C14	1.398	C19–H35	1.093	S1–C9–C14	120.2	C14–C16–H30	119.3
C19–H33	1.095	C20–C22	1.393	C13–C9–C14	119.4	C6–C17–H31	120.0
C20–H36	1.084	C21–C22	1.396	C4–C10–C7	120.2	C20–C17–H31	119.7
C21–H37	1.084	C22–H38	1.084	C4–C10–H25	119.9	C6–C18–H32	118.7
C21–C18–H32	120.9	C12–C19–H34	111.4	C12–C19–H35	111.4	H34–C19–H35	108.2
C17–C20–C22	120.1	C17–C20–H36	119.8	C22–C20–H36	120.1	C18–C21–C22	120.0
C18–C21–H37	119.9	C22–C21–H37	120.2	C20–C22–C21	119.9	C21–C22H38	120.1
C20–C22–H38	120.0						

**Table 2.** DFT computed molecular properties of 4-4-MPTB from B<sub>3</sub>LYP/6-311 + +G(d, p) level of theory.

Property	Parameter	Property	Parameter
Dipole moment ( $\mu_D$ )	5.58 Debye	$\Delta E_{Gap}$	4.21 eV
Polarizability ( $\alpha$ )	40.24 Å <sup>3</sup>	Chemical potential ( $\mu$ )	−4.0857
Proton affinity (PA)	939.29 KJ/mol	Chemical hardness ( $\eta$ )	2.1038
Ionization energy (IE)	7.75 eV	Softness ( $\sigma$ )	0.2377
Electron affinity (EA)	0.54 eV	Electrophilic index ( $\omega$ )	3.9762
$\epsilon_{HOMO}$	−6.19 eV	Electronegativity ( $\chi$ )	4.0857
$\epsilon_{LUMO}$	−1.98 eV		

Global reactivity descriptors provide a condensed overview of molecule's overall reactivity, bypassing the intricacies of specific reaction mechanisms. These descriptors prove invaluable to chemists, providing a swift and convenient means of comparing and contrasting the reactivity of different molecules. They enable the prediction of reaction likelihood and serve as a guide for designing new molecules with desired chemical properties.<sup>[30,31]</sup> Frontier molecular orbitals, namely HOMO and LUMO, play a pivotal role in comprehending molecule's chemical reactivity. A high HOMO-LUMO energy gap indicates reduced electron susceptibility to move from HOMO to LUMO, rendering the molecule less reactive and more stable. Conversely, a smaller gap suggests easier electron transfer, resulting

in higher reactivity for bond formation. Reactivity is contingent upon the ease of gaining or losing electrons, and descriptors such as ionization potential and electron affinity quantify the energy required for these processes. Chemical potential ( $\mu$ ) signifies a molecule's inclination to gain or lose electrons to attain a more stable state. Chemical hardness ( $\eta$ ) and chemical softness ( $\sigma$ ) encapsulate a molecule's resistance to changes in its electron configuration. Likewise, electrophilicity index ( $\omega$ ) predicts a molecule's electrophilic strength, indicating its ability to accept electrons. Electronegativity ( $\chi$ ) on the other hand measures an atom's propensity to attract electrons towards itself, reflecting its electron-attracting nature.

## 2.2. Vibrational Analysis

### 2.2.1. IR Spectra

Infrared (IR) spectroscopy measures molecular vibrations, which originates from the stretching and bending of chemical bonds. This technique directly observes functional groups by detecting the stretching and bending of bonds rather than intrinsic properties of the atoms themselves. Each bond type exhibit a distinction vibration frequency, leading to a unique peak in the IR spectrum. IR spectra are straightforward absorption spectra, with the x-axis depicting wavenumber ( $\text{cm}^{-1}$ ) representing the vibration frequency, and the y-axis indicating absorbance, reflecting the intensity of absorbed IR radiation. Computational calculations based on the B<sub>3</sub>LYP/6-311++G(d,p) DFT are conducted for frequency analysis and the spectroscopic signature of the 4-4-MPTB molecule. Theoretical calculations reveal that the molecule possesses C<sub>1</sub> point group symmetry, with its 38 atoms contributing to 108 modes of fundamental vibrations. The observed IR spectra for 4-4-MPTB and the experimentally obtained spectra are illustrated in Figures 2(a) and 2(b), respectively.

Analysis of the theoretical vibrational spectra revealed three prominent peaks within the 2000 and 1000  $\text{cm}^{-1}$  range. The peak at 1704  $\text{cm}^{-1}$  corresponds to C=O stretching, while peak at 1625  $\text{cm}^{-1}$  represents C=C double bond stretching. A sharp peak is observed at 1287  $\text{cm}^{-1}$  indicates skeletal C–C vibrations. On the left side of the spectrum, smaller absorption peaks with lower intensity are observed at around 3000  $\text{cm}^{-1}$ , primarily due to C–H stretching. The region below 1200  $\text{cm}^{-1}$  generally called 'fingerprint region' and not interpreted in detail as it contains single bonds (weaker) mostly involving atoms with higher mass. In this region, where single bond vibrations occur (e.g., C–S stretching), the molecule exhibits a multitude of peaks with low intensity. IR spectroscopy also quantifies the strength of a bond. The investigated molecule displays numerous peaks (low intensity) in the fingerprint region along with the information about the presence of double bonds and the precise position of C=O absorptions. Experimentally observed IR spectra<sup>[15]</sup> of 4-4-MPTB is depicted in Figure 2(b). The absorption peaks at 1704, 1625, and 1287  $\text{cm}^{-1}$  from theoretical calculations align with the experimental peaks of 1650, 1580, and 1280  $\text{cm}^{-1}$ , respectively. The position of the peaks at 3000  $\text{cm}^{-1}$  and in the fingerprint region are also corroborate with the experimental

confirmation. Tokyo Kasei Kogyo Company, Ltd,<sup>[32]</sup> demonstrated C=O, and C=C peaks at 1650, and 1586  $\text{cm}^{-1}$ , consistent with the DFT-computed IR spectra shown above.

### 2.2.2. NBO

Conjugation and delocalization play pivotal roles in influencing the photoinitiating properties of a molecule through various mechanisms. Conjugated systems with extended  $\pi$ -orbitals facilitate efficient overlap with incident light of specific wavelengths, resulting in enhanced light absorption crucial for initiating photochemical reactions. NBO analysis of 4-4-MPTB unveils intramolecular interactions, including hydrogen bonding and hyper-conjugative interactions, which impact molecular stability and chemical reactivity.<sup>[33]</sup> These insights provide a deeper understanding of electron density distribution and charge transfer within the molecule. Within the molecular structure of 4-4-MPTB, intriguing patterns of electron delocalization emerge. Natural atomic charges on S (+0.3023) and C5 (+0.5789) atoms indicate their susceptibility to nucleophilic attack. Similarly, notably negative charges on O2 (−0.5602) and C19 (−0.5910) compared to other atoms make them prone to electrophilic attack. The electron delocalization primarily arises from the conjugation of  $\pi$ -electrons across aromatic rings and the S atom within the molecule. NBO analysis indicates strong interactions between antibonding orbitals of C4–C11 with corresponding antibonding orbitals of C3–C8 and C7–C10, resulting in the highest energy interactions at 243.22 and 145.30 Kcal/mol, providing significant stabilization. Similarly, C9–C13 exhibits strong interactions with C14–C16 and C12–C15 anti-bonding  $\pi$ -orbitals, with stabilisation energy of 233.48 and 198.25 Kcal/mol, respectively. These above donor-acceptor interactions (filled and empty NBO's) are identified based on the highest stabilization energy, as determined by second-order perturbation theory analysis of the Fock matrix.

$$E(2) = \Delta E_{ij} = q_i \frac{F(i,j)^2}{\varepsilon_j - \varepsilon_i} \quad (5)$$

In the present equation,  $q_i$  represents the donor orbital occupancy,  $\varepsilon_i$  and  $\varepsilon_j$  are the diagonal elements (orbital energies), and  $F(i,j)^2$  denotes the off-diagonal NBO Fock matrix element. The stabilization energy  $E(2)$  is a measure of electron

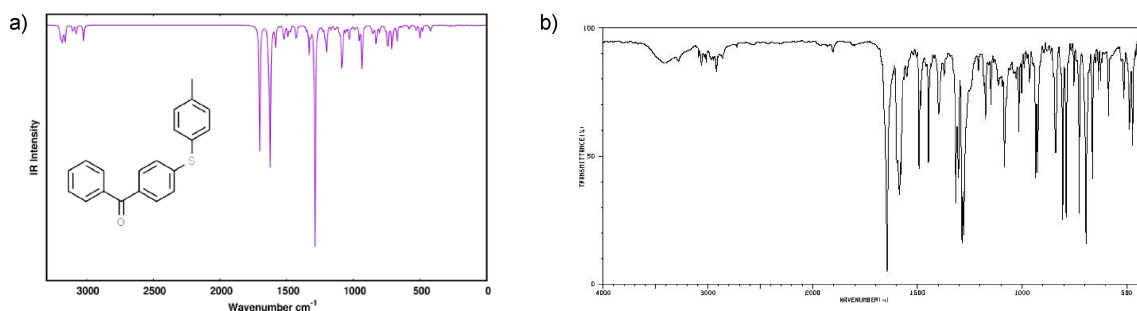


**Figure 2.** (a) DFT computed IR spectra of 4-4-MPTB molecule. (b) Experimentally reported IR spectra of 4-4-MPTB.<sup>[15]</sup>

delocalization estimation. Notably, the lone pair on S, characterized by the lowest occupancy and highest energy, primarily delocalizes into the anti-bonding  $\pi$ -orbitals of adjacent C4–C11, C9–C14, and C9–C13 bonds. Conversely, the lone pair of electrons on O atom draw very little stabilization energy (18 Kcal/mol) when interacting with nearby antibonding C3–C5 and C5–C6 orbitals. The observed electron delocalization in 4-4-MPTB significantly contributes to its stability and photoinitiating properties.

### 2.2.3. UV/Vis Spectra

UV/Vis spectroscopy is employed to scrutinize electronic transitions in both organic and inorganic molecules upon absorption of UV or visible light. This method measures the wavelength and intensity of absorbed UV and visible light, providing insights into the electronic structure of the sample molecule.<sup>[34]</sup> The absorption of radiation results in the promotion of electrons from the ground state to the excited state within the functional group referred to as the 'chromophore'. Each transition occurs between specific energy levels (molecular orbitals), giving rise to peaks in the spectrum. The low energy electronic excited states of 4-4-MPTB molecule are assessed using B<sub>3</sub>LYP/6-311++G(d,p) DFT theory. Gas-phase TD-DFT calculations are executed in the singlet state, considering the previously optimized ground-state geometry of the molecule. The calculated UV/Vis spectra of 4-4-MPTB molecule is depicted in Figure 3(a). The molecule exhibits a robust transition for the 2nd excited state at a wavelength 322.78 nm, with an oscillator strength (f) of 0.3616. The highest wave function coefficient for this electronic transition 80→81 corresponds to a nonbonding (n) orbital, typically found on lone pairs, transitioned to  $\pi$ -antibonding ( $n \rightarrow \pi^*$ ) molecular orbital.  $n \rightarrow \pi^*$  transitions require less energy to excite the electrons, resulting in absorption peaks appearing at longer wavelength. The second-highest peak coincides with the excited state 8 at a wavelength 258.09 nm, with an oscillator strength of 0.1345. The wave function coefficient for the transition which goes from 75→81 composed of  $\pi \rightarrow \pi^*$  orbitals. Electronic transitions such as  $\pi \rightarrow \pi^*$  commonly occur in conjugated systems like double

bonds or aromatic rings and typically occur in the UV or blue region.  $n \rightarrow \pi^*$  transitions generally manifest in the visible region (purple to red). Higher energy transitions (shorter wavelengths) require more energy and are weaker, resulting in smaller peaks. Higher absorbance or molar extinction coefficient indicates stronger transitions. The investigated molecule can absorb light in the quartz UV region and visible region. Molecules with extended conjugated- $\pi$  systems display absorption peak shifting to the higher wavelength regions. In conjugated- $\pi$  systems, the HOMO-LUMO gap decreases, causing absorption to occur in the visible region rather than the UV region. Table 3 showcases the molecular orbitals contributing the electronic transitions, especially  $n \rightarrow \pi^*$  and  $\pi \rightarrow \pi^*$  excited electronic transitions. The molecules that show delocalization of  $\pi$ -electrons, the absorption in such molecules shifts to longer wavelengths. Therefore, absorption requires less energy as the amount of delocalization increases. There must be less energy gap between bonding and anti bonding orbitals as a result the wavelength absorbed will eventually be high enough to be in the visible region of the spectrum and the molecule will then be seen as coloured. The significant delocalization in 4-4-MPTB places the molecule in the visible region, with a wavelength 322.78 nm.

### 2.2.4. UV/Vis Spectra in Solvent

When it comes to analyzing molecules using UV-Vis spectroscopy, understanding the solvent's influence is crucial. Water, as a highly polar (dielectric constant~80) and hydrogen-bonding solvent, significantly affects the UV-Vis spectra of molecules compared to studies in gas phase or non-polar environments.<sup>[35]</sup> Solvents with higher polarity values stabilize solute molecules due to increased solvent-solute interactions, leading to a decrease in energy difference between electronic states. This translates to red shifts (longer wavelengths) in the absorption maxima observed in the UV-Vis spectrum. 4-4-MPTB molecule shows  $\pi \rightarrow \pi^*$  transitions in the 2nd excited state (74→81) while two band of  $n \rightarrow \pi^*$  transitions (78→81 and 80→81) as shown in Figure 3(b). Aqueous medium incorporation leads to lowering the transition energy consequently increasing the

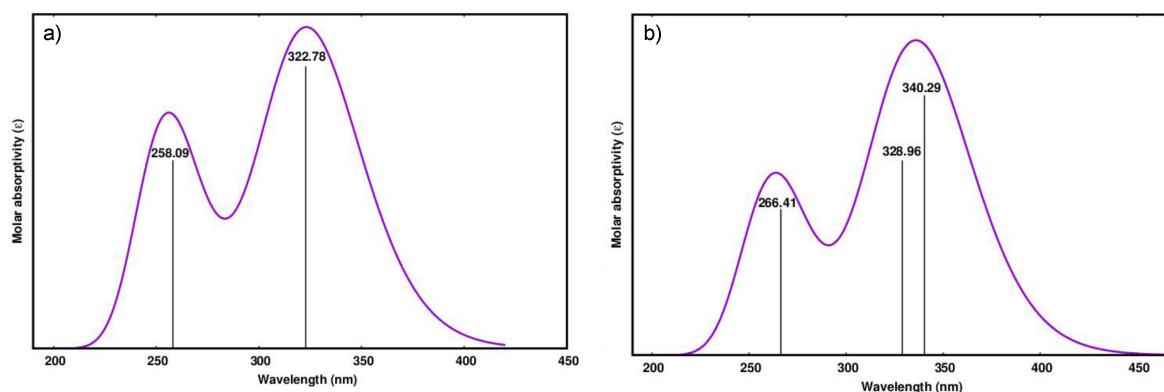
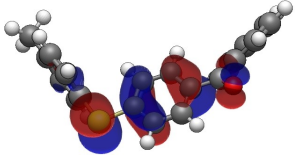
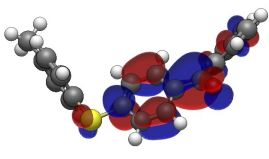
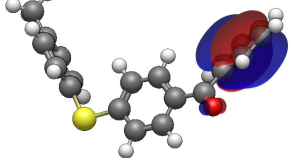
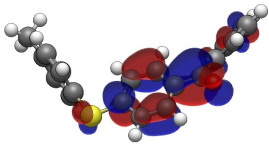


Figure 3. (a) UV/Vis spectra of 4-4-MPTB molecule in gas phase. (b) UV/Vis spectra of 4-4-MPTB molecule in aqueous medium.

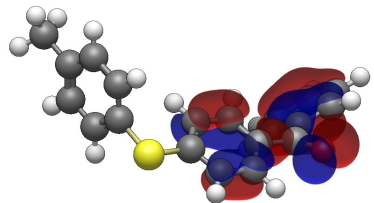
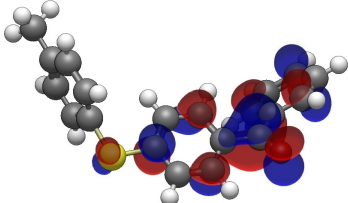
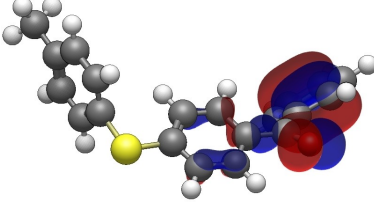
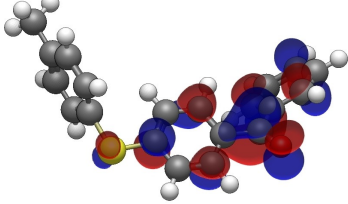
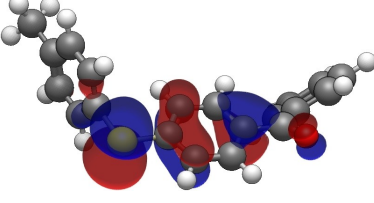
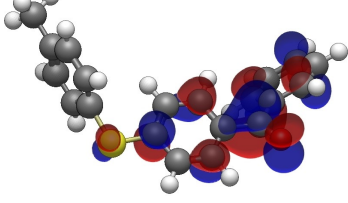
**Table 3.** DFT computed excited electronic state properties of 4-4-MPTB in gas phase.

Excitation energies and oscillator strengths		
$\pi \rightarrow \pi^*$ 75 $\rightarrow$ 81 f = 0.1345 E <sub>exc</sub> = 4.80 eV $\lambda$ = 258.09 nm	$\pi$ -bonding 	$\pi^*$ -antibonding 
$n \rightarrow \pi^*$ 80 $\rightarrow$ 81 f = 0.3616 E <sub>exc</sub> = 3.84 eV $\lambda$ = 322.78 nm	$n$ -non bonding 	$\pi^*$ -antibonding 

wavelengths of transitions which corresponds to visible region.  $\pi \rightarrow \pi^*$  transition corresponds to a wavelength of 266.41 nm while  $n \rightarrow \pi^*$  can be seen in two bands in the excited states with wavelengths 328.96 and 340.29 nm, respectively. Water's high dielectric constant significantly impacts electronic transitions in solutes. Polar solvents, for example water, often induce bathochromic shifts. In water, this is seen for n-donors like lone pairs on O, N, or S atoms. Polar solvents can enhance peak

intensity due to increased stabilization of the excited state through solvation, while non-polar solvents generally lead to weaker intensities. A higher intensity peaks are observed in solvents as compared to gas phase for 4-4-MPTB. Table 4 summarises important excited state transitions with energies, oscillator strengths, and wavelengths. UV/Vis spectra of the studied molecule is also obtained in relatively less polar solvents, such as ethanol and acetone, see Figures 4(a) and

**Table 4.** DFT computed excited electronic state properties of 4-4-MPTB in aqueous medium.

Excitation energies and oscillator strengths		
$\pi \rightarrow \pi^*$ 74 $\rightarrow$ 81 f = 0.1489 E <sub>exc</sub> = 4.65 eV $\lambda$ = 266.41 nm	$\pi$ -bonding 	$\pi^*$ -antibonding 
$n \rightarrow \pi^*$ 78 $\rightarrow$ 81 f = 0.1749 E <sub>exc</sub> = 3.77 eV $\lambda$ = 328.96 nm	$n$ -non bonding 	$\pi^*$ -antibonding 
$n \rightarrow \pi^*$ 80 $\rightarrow$ 81 f = 0.3140 E <sub>exc</sub> = 3.64 eV $\lambda$ = 340.29 nm	$n$ -non bonding 	$\pi^*$ -antibonding 

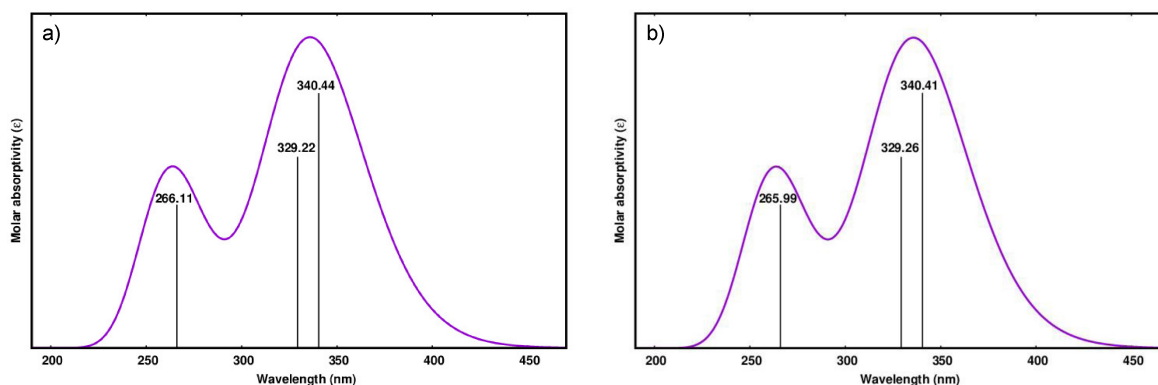


Figure 4. (a) UV/Vis spectra of 4-4-MPTB molecule in ethanol. (b) UV/Vis spectra of 4-4-MPTB molecule in acetone.

Table 5. Comparison of electronic excited state spectra and corresponding wavelength (nm), excitation energy (eV), and oscillator strength of 4-4-MPTB in different solvents.

Spectra	Water	Ethanol	Acetone
	$\lambda$ $E_{\text{exc}}$ $f$	$\lambda$ $E_{\text{exc}}$ $f$	$\lambda$ $E_{\text{exc}}$ $f$
$\pi \rightarrow \pi^*$	266.41 4.6538 0.1489	266.11 4.6591 0.1517	265.99 4.6613 0.1516
$n \rightarrow \pi^*$	340.29 3.6435 0.3140	340.44 3.6419 0.3022	340.41 3.6422 0.2955
	328.96 3.7690 0.1749	329.22 3.7660 0.1895	329.26 3.7655 0.1951

4(b). All the solvents introduce a bathochromic shift in  $n \rightarrow \pi^*$  transitions and hence the observed spectra move towards longer wavelengths, i.e. red shift. Similarly, in  $\pi \rightarrow \pi^*$  transitions, the observed spectra shows increase in energy upon changing the solvent from water to ethanol and acetone which leads hypsochromic shift, i.e. the spectra move towards lower wavelength (blue shift). In other words,  $\pi \rightarrow \pi^*$  transitions show blue shift while  $n \rightarrow \pi^*$  transitions show red shift in the spectra when polarity of the solvent is decreased. Excitation energies and corresponding wavelengths of  $n \rightarrow \pi^*$  transitions and  $\pi \rightarrow \pi^*$  transitions are shown in Table 5. Solvent effect is clearly seen in excited electronic state transitions; higher intensity peaks and bathochromic shifts corresponding figures and tables provide a richer understanding of the fascinating world of solvent effects in UV-Vis spectrometry.<sup>[36]</sup>

### 3. Conclusions

Using  $B_3LYP/6-311++G(d,p)$  method, DFT calculations were employed to evaluate the molecular and excited state electronic properties of 4-4-MPTB, a benzophenone derivative. The study involved a detailed analysis of chemical and reactivity attributes influencing its photoinitiating properties. Chemical reactivity parameters, including chemical potential ( $\mu$ ), chemical hardness ( $\eta$ ), softness ( $\sigma$ ), electrophilic index ( $\omega$ ), and electronegativity ( $\chi$ ), were computed using HOMO-LUMO energies based on Koopmans' approximation. Notably, 4-4-MPTB exhibited high dipole moment and polarizability values, indicative of strong intramolecular attractions and enhanced interactions. The low HOMO-LUMO gap suggested high chemical reactivity,

facilitating electron transfer from HOMO to LUMO orbitals, as indicated by global reactivity parameters.

Vibrational spectra revealed robust peaks at 1625 and 1704  $\text{cm}^{-1}$  for C=C and C=O stretching, consistent with experimental findings, alongside a sharp peak at 1287  $\text{cm}^{-1}$  representing skeletal C-C vibrations. UV/Vis spectra in gas phase exhibited excited state electronic transitions in the quartz UV and visible region, with notable peaks observed at 258.09 and 322.78 nm. Conjugation and delocalization were observed to reduce the energy gap between occupied and unoccupied electronic states, shifting absorption towards longer wavelengths in the visible region.

Absorption spectra in aqueous solvent showed peaks of excited electronic states with increased intensity and a shift towards longer wavelengths due to strong solvent-solute interactions. Comparative analysis with less polar solvents, such as ethanol and acetone, exhibited a bathochromic shift in  $n \rightarrow \pi^*$  transitions while hypsochromic shift in  $\pi \rightarrow \pi^*$  transitions, moving the spectra towards lower energy (longer wavelengths) and higher energy (shorter wavelengths), respectively. In summary, benzophenone-based photoinitiators remain vital in photopolymerization technology, with current research shedding light on solute behavior, solvent interactions, and intriguing molecular interactions revealed through UV-Vis spectrometry.

### 4. Declarations

#### 4.1. Ethical Approval

Not applicable

## 4.2. Funding

Not applicable

## Author Contributions

Not applicable

## Conflict of Interests

The authors declare no conflict of interest.

## Data Availability Statement

Data is available on request from the author.

**Keywords:** Benzophenones · photoinitiators · UV/Vis spectra · photopolymerization · DFT · chemical reactivity

- [1] T. L. Huang, Y. H. Li, Y. C. Chen, *J. Polym. Sci.* **2020**, *58*, 2914–2925.
- [2] W. Qianghua, Q. Baojun, *Polym. Eng. Sci.* **2001**, *41*, 1220–1226.
- [3] U. Altuntaş, V. Hitay, B. Özçelik, *Packag. Technol. Sci.* **2016**, *29*, 513–524.
- [4] T. Suzuki, S. Kitamura, R. Khotia, K. Sugihara, N. Fujimoto, S. Ohta, *Toxicol. Appl. Pharmacol.* **2005**, *203*, 9e17.
- [5] C. Feng, Q. L. Wang, F. Liu, B. Zhang, *Chem. Select* **2023**, *8*, e202302572.
- [6] R. Liska, *ChemPhysChem* **2011**, *12*, 1389–1389.
- [7] T. L. Huang, Y. C. Chen, *J. Photochem. Photobiol. A* **2022**, *429*, 113900.
- [8] I. Jimenez-Díaz, A. Zafra-Gomez, O. Ballesteros, A. Navalon, *Talanta* **2014**, *129*, 448e58.
- [9] B. Żaneta, T. Igor, G. Paweł, B. Beata, S. Alicja, M. Alicja, K. Grzegorz, B. Bogusława, *Reprod. Toxicol.* **2023**, *120*, 108450.
- [10] T. Gokhan, E. Burak, A. Meral, K. B. Demet, A. Nergis, *J. Photochem. Photobiol. A* **2011**, *219*, 26–31.
- [11] T. L. Huang, Y. H. Li, Y. C. Chen, *J. Polym. Sci.* **2020**, *58*, 2914–2925.
- [12] W. Ying, X. Pu, Q. W. Gang, Q. S. Su, N. Jun, *Chin. Chem. Lett.* **2007**, *18*, 977–980.
- [13] T. L. Huang, Y. C. Chen, *J. Photochem. Photobiol. A* **2022**, *429*, 113900.
- [14] K. Ramirez, E. Orrantia-Borunda, N. Flores, *J. Theor. Comput. Chem.* **2017**, *16*, 1750019.
- [15] Chemical Book, 4-(4-Methylphenylthio)benzophenone, [https://www.chemicalbook.com/SpectrumEN\\_83846-85-9\\_IR1.htm](https://www.chemicalbook.com/SpectrumEN_83846-85-9_IR1.htm), (Accessed 20 December 2023).
- [16] R. Aravindhan, H. Jianping, M. U. Momeen, *RSC Adv.* **2023**, *9*, 13(42), 29489–29495.
- [17] T. Giovannini, F. Egidi, C. Cappelli, *Chem. Soc. Rev.* **2020**, *49*, 5664–5677.
- [18] A. Bendjeddou, T. Abbaz, A. Gouasmia, D. Villemain, *Acta Chim. Pharm. Indica.* **2016**, *6*, 32–44.
- [19] L. Mendoza-Huizar, *Química Nova.* **2015**, *38*, 71–76.
- [20] M. Biswarup, S. Umasankar, R. D. Bhudeb, *Indian J. Adv. Chem. Sci.* **2016**, *4*(4), 401–408.
- [21] C. Lee, W. Yang, R. G. Parr, *Phys. Rev. B* **1988**, *37*, 211–212.
- [22] M. J. Frisch, G. W. Trucks, H. B. Schlegel, G. E. Scuseria, M. A. Robb, J. R. Cheeseman, G. Scalmani, V. Barone, G. A. Petersson, H. Nakatsuji, X. Li, M. Caricato, A. V. Marenich, J. Bloino, B. G. Janesko, R. Gomperts, B. Mennucci, H. P. Hratchian, J. V. Ortiz, A. F. Izmaylov, J. L. Sonnenberg, D. Williams-Young, F. Ding, F. Lipparini, F. Egidi, J. Goings, B. Peng, A. Petrone, T. Henderson, D. Ranasinghe, V. G. Zakrzewski, J. Gao, N. Rega, G. Zheng, W. Liang, M. Hada, M. Ehara, K. Toyota, R. Fukuda, J. Hasegawa, M. Ishida, T. Nakajima, Y. Honda, O. Kitao, H. Nakai, T. Vreven, K. Throssell, J. A. Montgomery, J. E. Peralta, F. Ogliaro, M. J. Bearpark, J. J. Heyd, E. N. Brothers, K. N. Kudin, V. N. Staroverov, T. A. Keith, R. Kobayashi, J. Normand, K. Raghavachari, A. P. Rendell, J. C. Burant, S. S. Iyengar, J. Tomasi, M. Cossi, J. M. Millam, M. Klene, C. Adamo, R. Cammi, J. W. Ochterski, R. L. Martin, K. Morokuma, O. Farkas, J. B. Foresman, D. J. Fox, *Gaussian 16 Revision C.01*, Gaussian Inc. Wallingford CT, **2016**.
- [23] G. Duca, N. Bolocan, *Rev. Chim.* **2021**, *72*(4), 162–174.
- [24] J. Singar, *Res. Chem. Intermed.* **2020**, *46*, 2457–2479.
- [25] A. M. Ellis, C. A. Mayhew, In *Proton Transfer Reaction Mass Spectrometry Principles and Applications*; John Wiley & Sons, Chichester, United Kingdom: **2014**.
- [26] T. Koopmans, *Physica* **1934**, *1*, 104–110.
- [27] S. Selvaraj, P. Rajkumar, M. Kesavan, S. Gunasekaran, S. Kumaresan, *J. Mol. Struct.* **2018**, *1173*, 52–62.
- [28] V. Dixit, R. A. Yadav, *Int. J. Pharm.* **2015**, *491*, 277–284.
- [29] P. K. Chattaraj, U. Sarkar, D. R. Roy, *Chem. Rev.* **2006**, *106*, 2065–2091.
- [30] V. Balachandran, S. Rajeswari, S. Lalitha, *Spectrochim. acta. Part A, Mol. biomol. spectrosc.* **2013**, *101*, 356–369.
- [31] S. Muthu, S. Renuga, *Spectrochim. acta. Part A, Mol. biomol. spectrosc.* **2014**, *118*, 683–694.
- [32] SpectraBase, Tokyo Kasei Kogyo Company, Ltd., Tokyo, Japan, <https://spectrabase.com/spectrum/ELVtqpdL>, (Accessed 20 December 2023).
- [33] L. Padmaja, C. Ravikumar, D. Sajan, I. H. Joe, V. S. Jayakumar, G. Pettit, O. F. Nielsen, *J. Raman Spectrosc.* **2009**, *40*(4), 419–428.
- [34] R. Rijal, M. Sah, H. P. Lamichhane, *Heliyon.* **2023**, *21.9*(3), e14801.
- [35] L. Wenbo, L. Qianru, W. Xiaofeng, H. Liping, M. Yanbin, W. Yashi, L. Jianhuang, Z. Can, W. Liying, L. Mengfen, B. Zhijian, *J. Phys. Conf. Ser.* **2021**, *2011*, 012103.
- [36] T. Shota, S. Bikramjit, N. Masanari, H. Christof, *J. Phys. Chem. A* **2021**, *125*(33), 7198–7206.

Manuscript received: February 17, 2024